

Characterization of the injectors near-field region of LRE combustion chambers

P. E. Lapenna^{*†}, *A. Remiddi*^{*}, *G. Indelicato*^{*}, *M. Valorani*^{*}, *M. Pizzarelli*^{**} and *F. Creta*^{*}

^{*} *Sapienza University of Rome, via Eudossiana 18 - 00184 Rome, Italy*

^{**} *Italian Space Agency, Via del Politecnico snc, 00133 Rome, Italy*

[†]*pasquale.lapenna@uniroma1.it*

[†]Corresponding author

Abstract

The injectors near-field region of LRE combustion chambers is numerically investigated by means of both multi and single-injector combustor simulations. An efficient and validated uRANS numerical framework based on non-adiabatic flamelets is used to describe methane-oxygen turbulent nonpremixed combustion. Two paradigmatic configurations, representing the flame-wall and flame-flame interactions occurring on an injection plate are used to develop a 2D axy-symmetric dataset. On both configurations, the confinement length of the injector is parametrically varied in order to isolate its effect on the heat flux insisting on the injector face-plate. Finally the results are compared to a fully 3D case, consisting in 37 injectors characterized by the same operating conditions and parameters as the 2D cases.

1. Introduction

In recent years, an ever increasing interest towards new propellants combinations for liquid rocket engines (LRE) has been observed. In particular the use of methane, in combination with liquid oxygen (LOx), as the fuel for high-performance, cost-effective and possibly reusable LREs has been largely explored from both space agency and private companies. In Europe, the more prominent activities on methane/oxygen based LRE are the M10 engine of the upper stage of the VEGA-E launcher^{16,22} and the Prometheus prototype for future launch systems, envisioned for the post-Ariane-6 phase. In the United States, in the context of the Morpheus program, NASA has developed a ~ 20 kN class methane/oxygen LRE prototype for planetary landing.²⁵ Concurrently, private companies such as SpaceX and Blue Origin have shown their interest in methane/oxygen LREs with the development of the Raptor and the BE-4 engines respectively. This being said, significant effort in such technologies has also been devoted outside of Europe and the United States as recently reported.^{2,17}

The motivations for this interest in such propellant combination are nowadays well-known since methane features the highest specific impulse among the fuels based on hydrocarbons.³² Such elevated performances come with additional advantages over the standard LRE fuels being soft-cryogenic⁴ which helps both the tank and the regenerative cooling system operations³⁶ where also a significant low rate of coking.²¹ In addition, methane is significantly more sustainable compared to other hydrocarbons as well as fuels based on hydrazine given its low-toxicity. Methane has also shown a limited propensity to produce soot during its oxidation at operating pressure of interest for LRE combustion chambers.²⁰

Given these premises, the development of variable-fidelity Computational Fluid Dynamics (CFD) tools capable of support experiments and the system design are of significant interest for the development of methane-fueled LREs. This being particularly true for the numerical prediction of the thermal loads in the combustion chamber which directly impact the rocket operating life as well as its re-usability. However, the numerical modeling of the flow inside a LRE combustion chamber is still nowadays an extremely difficult task being such flow multi-scale, multi-physics as well as occurring in a complex geometrical configuration. As a result, complete numerical characterization of the combustion chambers have not been carried out and usually full-scale simulations have been focused on particular aspect, such as for instance the combustion instability.³⁷

Regarding the thermal characterization of LRE combustion chamber, the vast majority of the numerical simulations have been devoted to the investigation of the lateral part of the combustion chamber, as well as the nozzle sections.³ This being mainly motivated by the fact the operating life of a LRE is typically assumed to be governed by the thermal loads in the throat region.^{29,30} More recently, additional research efforts have been focused on the entire thrust chamber system and, in particular, numerical investigations of the firing plate region are expected to be of great

CHARACTERIZATION OF INJECTORS NEAR-FIELD IN LRE

interest from both scientific and technical standpoints. A comprehensive investigation of the thermal loads in the injection region is still lacking in the literature although some works can be found on the effects of the injector layout on different configurations.^{1,38}

In this context, the present contribution is focused on the numerical characterization of the injectors near-field region of LRE combustion chambers employing methane/oxygen as propellants. The main idea is to understand the role of injector lateral confinement distance in a firing plate by means of a thorough parametric analysis following some previous contributions.^{33,34} The parametric analysis consists in a number of 2D axis-symmetric unsteady Reynolds averaged Navier Stokes (uRANS) simulations using a recently proposed approach.¹² The ensuing data are then compared to a 37-injector injection plate developed, mainly for this comparison, using the same reference injector parameters. The reference baseline case is the gaseous oxygen (GOx) and gaseous methane (GCH4) single injector combustor developed at the Technical University of Munich (TUM).^{5,27} This case has been largely investigated by many groups using both RANS^{6,26,28} and Large Eddy Simulations (LES),^{7,23,39} therefore providing a good starting point for our work.

2. Methods

2.1 Numerical Framework

In this work, a well established pressure-based solver is employed featuring non-adiabatic steady laminar flamelets as the thermochemical manifold. This solver is based on the open-source numerical frameworks of OpenFOAM and OpenSMOKE++⁸ and it has been successfully applied to a number of different combustion chambers configurations.^{11,13–15,18,19} For the present investigation the same models as well as settings of the work by Indelicato et al.¹² are used since the baseline case selected is in both cases the TUMrig single injector chamber.⁵ As a result, also the flamelet libraries, i.e the thermochemical manifolds, are exactly the same as in,¹² for this reason they are briefly described in the following paragraph. Steady laminar flamelet solutions have been obtained resorting to the GRI3.0 chemical mechanism³⁵ while the flamelet tables, needed at run-time by the CFD solver, have the following structure:

$$\tilde{\psi} = \tilde{\psi}(\tilde{Z}, \tilde{Z}'^2, \tilde{\chi}_{st}, \tilde{\phi}) \quad (1)$$

where $\tilde{\psi}$ is a generic Favre-averaged thermochemical variable. The latter is looked-up during the simulation as a function of: the average mixture fraction \tilde{Z} , the mixture fraction variance \tilde{Z}'^2 , the stoichiometric scalar dissipation rate $\tilde{\chi}_{st}$ and the enthalpy defect $\tilde{\phi}$. As described by Lapenna et al.,¹⁹ for \tilde{Z} , \tilde{Z}'^2 and $\tilde{\phi}$ additional transport equations are solved while for $\tilde{\chi}_{st}$ an algebraic relation is employed.³¹ The non-adiabatic effects occurring at the walls of the combustion chamber are taken into account by $\tilde{\phi}$ measuring the enthalpy that the reacting flow is losing due to the flame-wall interaction. The frozen chemistry assumption is used since it has shown to provide accurate results for the considered thermodynamic conditions.¹² While the original formulation comes from the work of Marracino and Lentini²⁴ in the context of luminous sooting nonpremixed flames. In order to take into account turbulence-chemistry interaction, the flamelet tables of Eq. 1, use a presumed pdf-approach where a beta-pdf is chosen for the subgrid scale statistics of the mixture fraction employing \tilde{Z} and \tilde{Z}'^2 as inputs. Conversely simple Dirac-delta distributions are used for the scalar dissipation rate and the enthalpy defect. Note that for simplicity the Favre averaging symbol $\tilde{\cdot}$ is dropped in the following sections.

Operatively, the mentioned uRANS solver employs a second order accuracy for spatial discretization and an implicit first order time integration scheme while the PIMPLE algorithm⁹ is used for pressure-velocity coupling. The standard $k - \epsilon$ model is used for turbulence closure in conjunction with a modified thermal wall function¹⁰ resulting in computationally affordable grid requirements at the walls. Additional details on the numerical formulation can be found in the recent work by Indelicato et al.¹²

2.2 Numerical configurations

As previously mentioned, the baseline reference case is the experimental shear coaxial GOx/GCH4 injector in the square-section TUMrig combustor. The injection parameters for all the simulations discussed in this work are taken from the work of Celano et al.,⁵ which correspond to a particular operating point of the combustor at a chamber pressure of 20 bar and a nominal oxidizer to fuel ratio of $O/F = 2.6$. As the 2D axis-symmetric approximation is used, the numerical domain considered is therefore a wedge of an equivalent cylindrical combustion chamber, with a chamber radius defined to guarantee the same mass-flux as the reference square-section experimental chamber as commonly done for RANS and uRANS.⁶

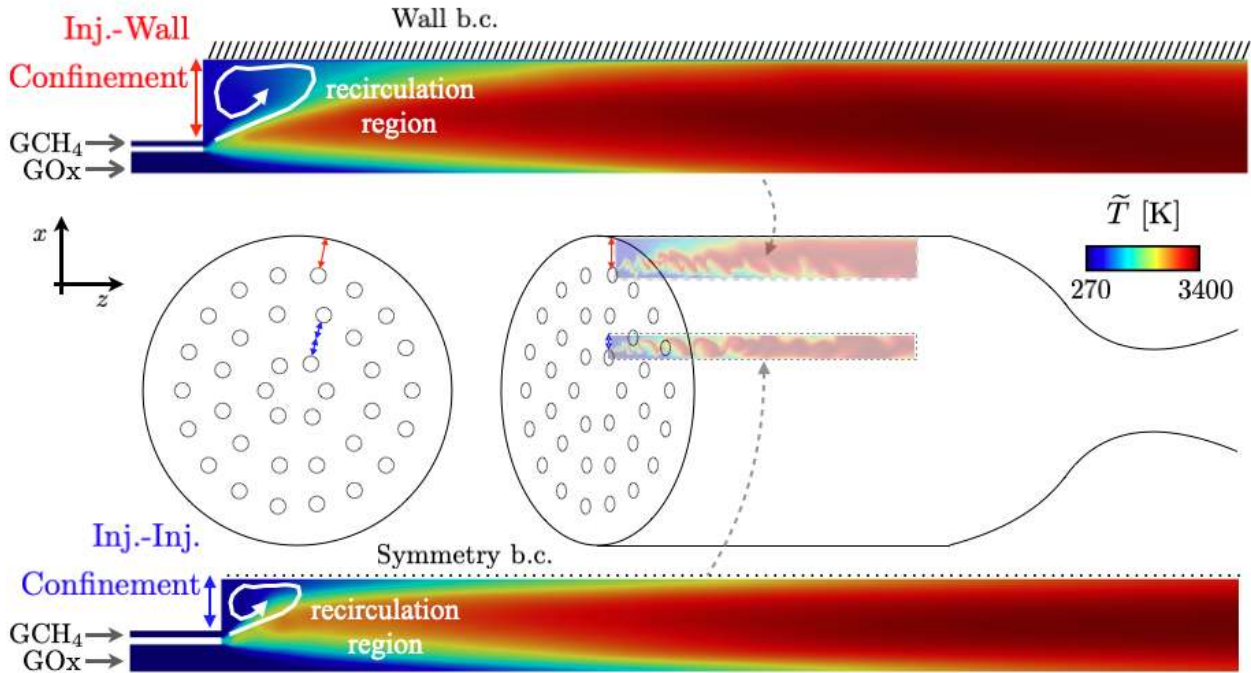


Figure 1: Schematic of the two paradigmatic 2D axis-symmetric configurations studied. Upper sub-figure: wall-bounded configuration representative of the injector-wall interaction. Lower sub-figure: symmetric configuration representative of the injector-injector interaction. In the central sub-figure the two configurations are reported on a hypothetical multi-dimensional problem with multiple injection elements. The color-coded fields represent time-averaged temperature in the upper and lower sub-figures while instantaneous temperature in the schematics of the central sub-figure (not to scale).

To emulate the different flame-flame and flame-wall interactions occurring within a generic multi-injector plate, two paradigmatic configurations have been considered as schematically reported in Fig. 1. Flame-wall interactions are investigated using a wall-bounded configuration while flame-flame interactions are investigated resorting to a symmetry plane instead of the wall boundary condition. The rationale behind this choices is reported in detail in two previous contributions.^{33,34}

From the CFD standpoint, given the intrinsic differences between the two configurations, grid convergence analysis have been conducted for both the cases in order to asses a baseline reference resolution. In addition, also the effect of the thermal boundary condition (b.c.) on the ensuing flow fields in the two configurations reported in Fig. 1 has been assessed. The end result of this analysis is the definition of the dataset conditions to investigate the confinement effects on the flame, flow field and on the ensuing thermal loads. In particular, the confinement length L_C has been parametrically varied between $0.5C$ and $2.5C$ being C its nominal value of $3.77 \cdot 10^{-3}$ m. The parametric analysis has been conducted for both the wall-bounded and symmetric configurations, and for each of them the fully-adiabatic and fully-isothermal sets of boundary conditions have been simulated, as reported in Tab. 1. Regarding the labels used, the first label letter indicates the configuration used (wall W or symmetry S b.c. of the lateral boundary) then the following two letters represent the thermal b.c. used respectively on the plate and lateral boundary (I for imposed temperature and A for adiabatic). Finally the normalized confinement length is given as XpXX, where for instance $L_C = 1.5C$ is labelled as 1p50.

Note that the parametric analysis is carried out by varying only the injection plate confinement length L_C , while keeping all the injector geometry and parameters fixed. The number of computational grid points employed in the transverse direction are changed accordingly in order to maintain a constant grid spacing.

CHARACTERIZATION OF INJECTORS NEAR-FIELD IN LRE

Table 1: Labels of the simulations carried out for the parametric analysis.

L_C/C	Wall - Isotherm. b.c.	Wall - Adiab. b.c.	Symmetry - Isotherm. b.c.	Symmetry - Adiab. b.c.
0.50	W-II-0p50	W-AA-0p50	S-I-0p50	S-A-0p50
0.75	W-II-0p75	W-AA-0p75	S-I-0p75	S-A-0p75
1.00	W-II-1p00	W-AA-1p00	S-I-1p00	S-A-1p00
1.25	W-II-1p25	W-AA-1p25	S-I-1p25	S-A-1p25
1.50	W-II-1p50	W-AA-1p50	S-I-1p50	S-A-1p50
1.75	W-II-1p75	W-AA-1p75	S-I-1p75	S-A-1p75
2.00	W-II-2p00	W-AA-2p00	S-I-2p00	S-A-2p00
2.25	W-II-2p25	W-AA-2p25	S-I-2p25	S-A-2p25
2.50	W-II-2p50	W-AA-2p50	S-I-2p50	S-A-2p50

3. Preliminary Results

3.1 Confinement parametric analysis

The dataset presented in the previous section is now preliminary analyzed in terms of time averaged values of some quantities of interest which are then spatially averaged on either the injection plate surface or the lateral chamber wall. The quantities of interest selected are the heat flux $\langle q \rangle$, heat transfer coefficient $\langle h_c \rangle$ and adiabatic flame temperature $\langle T_{ad} \rangle$.

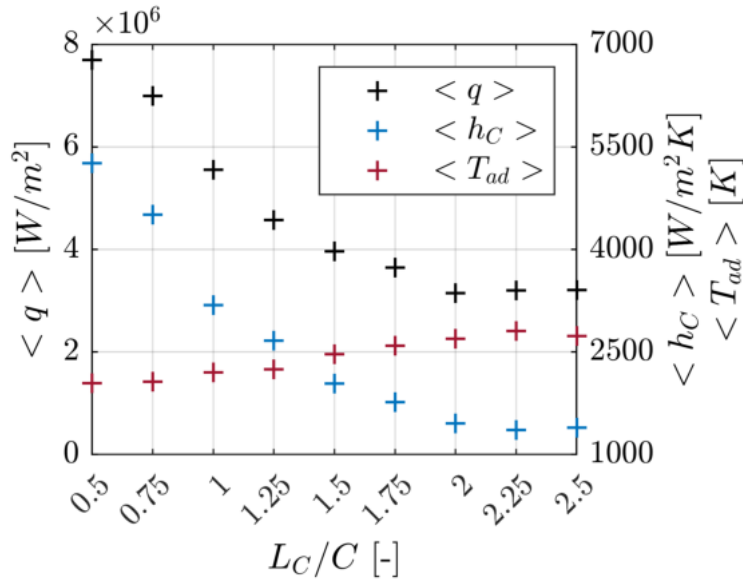


Figure 2: Time and surface averaged values of heat flux $\langle q \rangle$, heat transfer coefficient $\langle h_c \rangle$ and adiabatic flame temperature $\langle T_{ad} \rangle$ on the lateral wall as functions of the investigated confinement values.

Figure 2 shows the trend of the mentioned quantities of interest evaluated on the lateral wall as functions of the investigated confinement values. As the confinement length is increased the thermal power of the turbulent flame ensuing from the single injector is distributed on a larger surfaces of the lateral wall. As a result both the heat flux and the heat transfer coefficient decreases as the confinement is varied from $L_C/C = 0.5$ to $L_C/C = 2.0$. On the other hand, for the same range, the adiabatic flame temperature is increasing almost linearly with the L_C/C up to ~ 2500 [K].

Figure 3 shows, for the same simulations considered in Fig. 2, the trends of the quantities of interest evaluated on the injection plate wall as functions of the confinement length. It is observed that the heat flux insisting on the injection plate significantly increase with L_C/C showing an opposite trend compared to the lateral wall. Concurrently, the heat transfer coefficient decreases significantly up to ~ 1500 $\text{W/m}^2\text{K}$ due to the smaller increment of $\langle T_{ad} \rangle$ with increasing L_C/C .

Figure 4 displays, for the simulation featuring the symmetric b.c. on the lateral wall, the trends of the quantities of interest evaluated on the injection plate wall as functions of the confinement length. Similarly to the wall-bounded

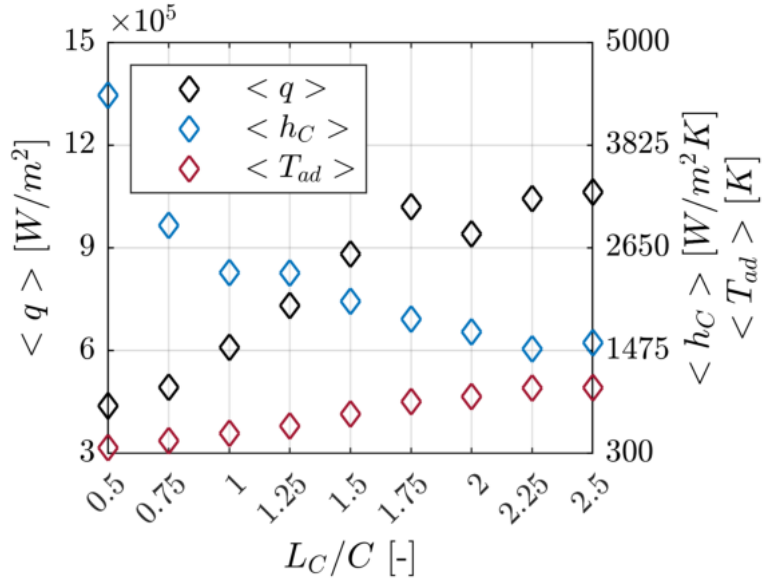


Figure 3: Time and surface averaged values of heat flux $\langle q \rangle$, heat transfer coefficient $\langle h_c \rangle$ and adiabatic flame temperature $\langle T_{ad} \rangle$ on the injector face-plate as functions of the investigated confinement values for the wall bounded simulations emulating the flame-wall interaction.

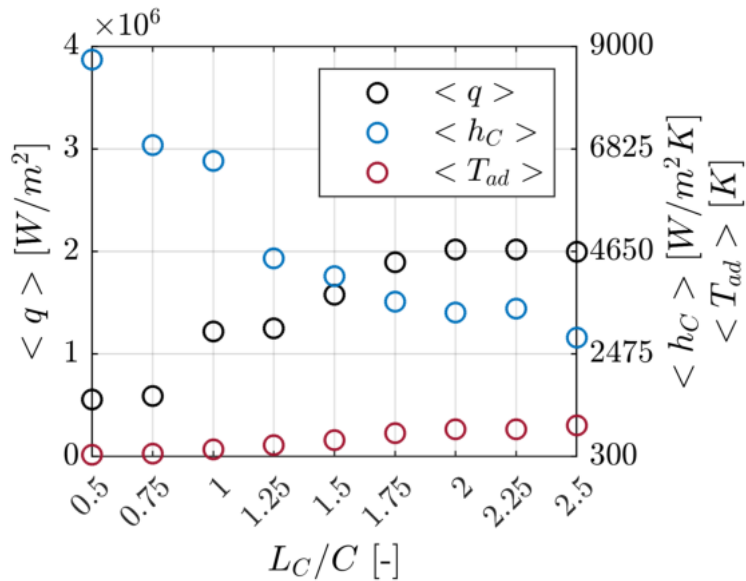


Figure 4: Time and surface averaged values of heat flux $\langle q \rangle$, heat transfer coefficient $\langle h_c \rangle$ and adiabatic flame temperature $\langle T_{ad} \rangle$ on the injector face-plate as functions of the investigated confinement values for the sym.-bounded simulations emulating the flame-flame interaction.

cases, the heat flux insisting on the injection plate increases with L_C/C however, reaching higher values up to 2 MW/m^2 . Similar conclusions can be drawn for $\langle h_c \rangle$ and $\langle T_{ad} \rangle$, although for different absolute values.

The increase of heat flux on the injection plate for both the configurations can be explained in terms of the interaction between the recirculation region and the mean flame as reported in Fig. 5. In particular, when the confinement is limited the recirculation region is mostly composed by cold methane coming from the injector while for large confinement lengths the recirculation region start to collect hot products from the flame. Such hot products are convected backward toward the injector face plate ultimately resulting in an elevated heat flux on such surface.

CHARACTERIZATION OF INJECTORS NEAR-FIELD IN LRE

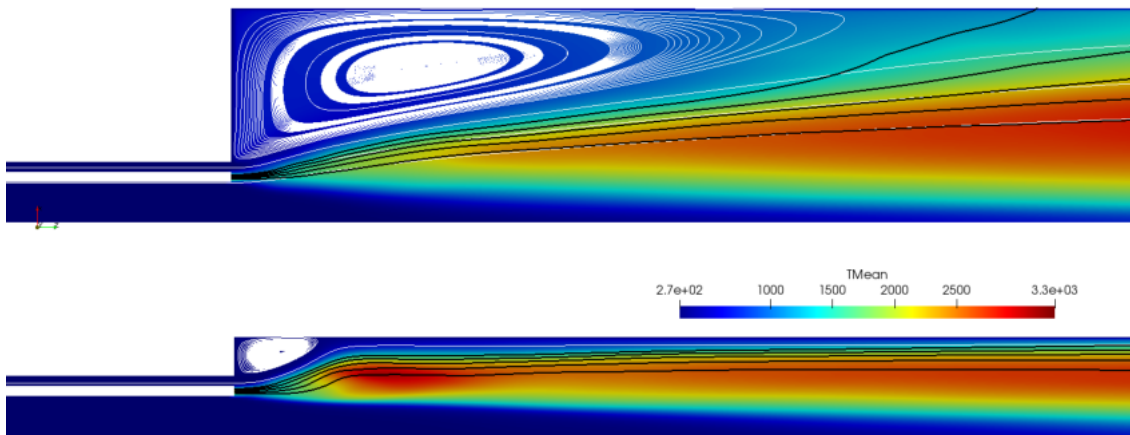


Figure 5: Interaction between the recirculating region (white lines, representing the stream lines) and the flame (black contours representing the average values of the mixture fraction).

3.2 Comparison with 3D case

The preliminary results obtained by means of the parametric analysis presented in the previous subsection have shed light on the effect of confinement on the thermal loads in the injection region. At this stage, it is now important to evaluate the soundness of the assumptions made for the 2D configurations using a reference 3D simulation. To this end a 37 injectors plate configuration has been developed as shown in Fig. 6, where the injection arrangement features a 15 degree symmetry.

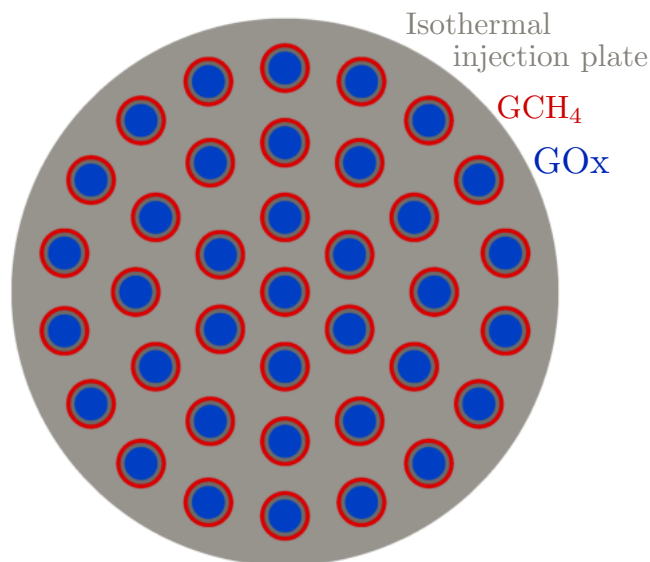


Figure 6: 37 injectors plate configuration using the same injectors parameters and operating conditions of the 2D cases.

As mentioned in the introduction all the injection parameters as well as the operating chamber conditions (hence the chamber pressure and the O/F) are identical to the experimental single-injector case.⁵ The chamber length is also the same as the baseline case together with temperature imposed as in the validation case presented by Indelicato et al.¹² On the firing plate the fuel injection temperature is imposed consistently with the 2D dataset.^{33,34} The simulation

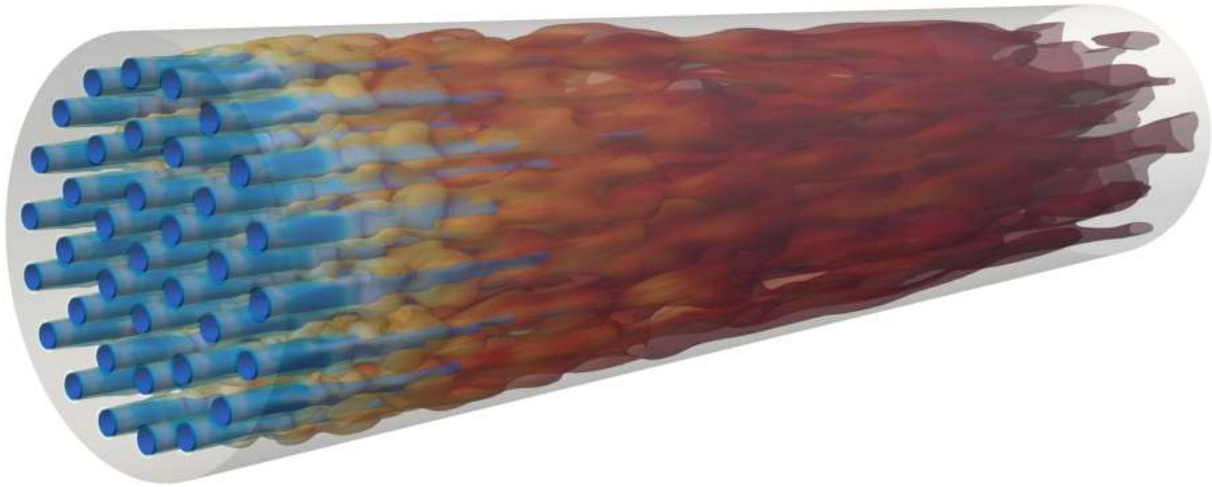


Figure 7: Instantaneous representation of multi-injector simulation employed for this work, the color coding on representative compositional iso-surfaces represents the temperature and varies from blue (reactants temperature) to dark red (adiabatic flame temperature).

is carried resorting to the same numerical strategy employed for the 2D cases with a computational grid consisting in 10 Millions finite volumes which is expected to correctly reproduce the main flow features as shown in Fig. 7. In addition, the ensuing y^+ values span from 100 to 700 falling well inside the admissible range for the thermal wall functions employed.¹²

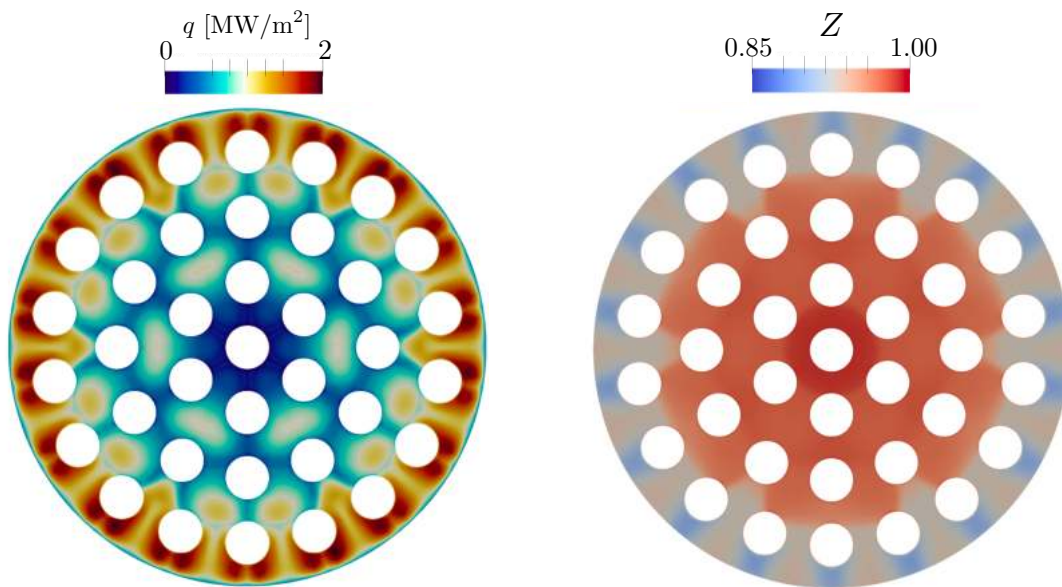


Figure 8: Time averages of the heat flux (left panel) and the mixture fraction (right panel) on the injection plate.

The resulting time averaged heat flux insisting on the injection plate is shown in Fig. 8, where the maximum heat flux experienced by the present 37-Injector configuration is $\sim 2 \text{ MW/m}^2$ consistently with the 2D simulations. In addition it is clearly observable that the internal part of the plate is characterized by lower values of the heat flux compared to the external injectors ring. This trend is partially explained by the distribution of the averaged mixture

CHARACTERIZATION OF INJECTORS NEAR-FIELD IN LRE

fraction on the plate which is also reported in Fig. 8. In particular, in the inner part of the injection plate a richer mixture is recirculating near the wall resulting in a colder flow.

4. Conclusion

In this contribution, a numerical investigation of the injectors near-field region of LRE combustion chambers has been carried out using both multi and single-injector combustor simulations. Numerical simulations of methane-oxygen turbulent combustion have been carried out resorting to an efficient uRANS approach. A 2D axy-symmetric dataset, consisting in two paradigmatic configurations, has been investigated in order to shed light on the role of the confinement length on the heat flux that insists on the injection plate. It has been shown that the heat flux on the injection plate increases with the confinement length irrespective of the interaction considered, either flame-wall (wall bounded b.c.) or flame-flame (sym.-bounded b.c.). This trend has been tentatively explained in terms of the interplay between the recirculation region and the turbulent flame ensuing from the injector. Using the same injector parameters a 37-injector combustion chamber has been developed and numerically investigated. Results consistent with the 2D dataset have been obtained in terms of maximum heat flux values on the injection plates. Future research effort will be devoted to a throughout comparison between the 2D and 3D results and to the development on data-driven surrogate models.

5. Acknowledgments

This research was jointly funded by Sapienza University and the Italian Space Agency - Agenzia Spaziale Italiana (ASI) as part of the research N.2019-4-HH.0 carried out under the framework agreement N.2015-1-Q.0 CUP:F86C17000080005.

References

- [1] Sherif Ahdy, Mohammed A Boraey, Hesham Abdel Hameed, and Hafez El Salmawy. Effect of the wall thermal boundary condition on the structure of a confined swirling diffusion flame. *Journal of the Brazilian Society of Mechanical Sciences and Engineering*, 41(11):1–12, 2019.
- [2] Hiroya Asakawa, Hideaki Nanri, Kenji Aoki, Isao Kubota, Hatsuo Mori, Yasuhiro Ishikawa, Kenichi Kimoto, Shinji Ishihara, and Shinichiro Ishizaki. *The status of the research and development of LNG rocket engines in Japan*. Springer, 2017.
- [3] Barbara Betti, Daniele Bianchi, Francesco Nasuti, and Emanuele Martelli. Chemical reaction effects on heat loads of CH₄/O₂ and H₂/O₂ rockets. *AIAA Journal*, 54(5):1693–1703, 2016.
- [4] Holger Burkhardt, Martin Sippel, Armin Herbertz, and Josef Klevanski. Kerosene vs. methane: a propellant tradeoff for reusable liquid booster stages. *Journal of Spacecraft and Rockets*, 41(5):762–769, 2004.
- [5] M. P. Celano, S. Silvestri, G. Schlieben, C. Kirchberger, O. J. Haidn, and O. Knab. Injector characterization for a gaseous oxygen-methane single element combustion chamber. *Progress in Propulsion Physics*, 8:145–164, 2016.
- [6] Alexander Chemnitz, Thomas Sattelmayer, Christof Roth, Oskar Haidn, Yu Daimon, Roman Keller, P Gerlinger, Julian Zips, and Michael Pfitzner. Numerical investigation of reacting flow in a methane rocket combustor: turbulence modeling. *Journal of Propulsion and Power*, 34(4):864–877, 2018.
- [7] Wai Tong Chung, Aashwin Ananda Mishra, Nikolaos Perakis, and Matthias Ihme. Data-assisted combustion simulations with dynamic submodel assignment using random forests. *Combustion and Flame*, 227:172–185, 2021.
- [8] A. Cuoci, A. Frassoldati, T. Faravelli, and E. Ranzi. Opensmoke++: An object-oriented framework for the numerical modeling of reactive systems with detailed kinetic mechanisms. *Computer Physics Communications*, 192:237–264, 2015.
- [9] Joel H Ferziger, Milovan Perić, and Robert L Street. *Computational Methods for Fluid Dynamics*, volume 3. Springer, 2002.
- [10] Zhiyu Han and Rolf D Reitz. A temperature wall function formulation for variable-density turbulent flows with application to engine convective heat transfer modeling. *International Journal of Heat Mass Transfer*, 40(3):613–625, 1997.

- [11] G Indelicato, P E Lapenna, R Concetti, M Caputo, M Valorani, G Magnotti, and F Creta. Numerical investigation of high pressure CO₂-diluted combustion using a flamelet-based approach. *Combustion Science and Technology*, 192(11):2028–2049, 2020.
- [12] G Indelicato, PE Lapenna, A Remiddi, and F Creta. An efficient modeling framework for wall heat flux prediction in rocket combustion chambers using non adiabatic flamelets and wall-functions. *International Journal of Heat and Mass Transfer*, 169:120913, 2021.
- [13] Giuseppe Indelicato, Pasquale E Lapenna, Nelson P Longmire, Arianna Remiddi, Daniel T Banuti, and Francesco Creta. Dataset of wall-resolved large eddy simulations turbulent pseudo-boiling in cryogenic hydrogen pipe flows. *Journal of Thermophysics and Heat Transfer (under review)*, 2022.
- [14] Giuseppe Indelicato, Arianna Remiddi, Pasquale E Lapenna, and Francesco Creta. Application of wall functions approaches in the context of LRE combustion chambers simulations. In *AIAA Paper 2021-1375*, August 2021.
- [15] Giuseppe Indelicato, Federico Vona, Arianna Remiddi, Pasquale E. Lapenna, and Francesco Creta. A flamelet-based numerical framework for the simulation of low-to-high mach number flows in Ire. August 2020.
- [16] D Kajon, C Boffa, P Vinet, M Rudnykh, D Drigo, L Arione, N Ierardo, and A Sirbi. Development status of the liquid oxygen and methane M10 rocket engine for the Vega-E upper stage. In *Proceedings of 7th Edition of the Space Propulsion Conference*, pages 1–7, 2021.
- [17] Jeong Soo Kim, Hun Jung, and Jong Hyun Kim. State of the art in the development of methane/oxygen liquid-bipropellant rocket engine. *Journal of the Korean Society of Propulsion Engineers*, 17(6):120–130, 2013.
- [18] P. E. Lapenna, G. Indelicato, R. Lamioni, and F. Creta. Modeling the equations of state using a flamelet approach in LRE-like conditions. *Acta Astronautica*, 158:460–469, 2019.
- [19] Pasquale E Lapenna, Ruggero Amaduzzi, Diego Durigon, Giuseppe Indelicato, Francesco Nasuti, and Francesco Creta. Simulation of a single-element GCH₄/GO_x rocket combustor using a non-adiabatic flamelet method. In *AIAA Paper 2018-4872*, July 2018.
- [20] Pasquale E Lapenna, Pietro P Ciottoli, and Francesco Creta. The effect of fuel composition on the non-premixed flame structure of lng/lox mixtures at supercritical pressure. *AIAA Paper 2016-0690*, January 2016.
- [21] Keming Liang, Baoe Yang, and Zhongli Zhang. Investigation of heat transfer and coking characteristics of hydrocarbon fuels. *Journal of Propulsion and Power*, 14(5):789–796, 1998.
- [22] D Liuzzi, P Tadini, A Terracciano, G Bianchi, M Sciarra, M Rudnykh, D Drigo, L Arione, N Ierardo, and A Sirbi. Development of an ALM thrust chamber for Vega-E M10 rocket engine. In *Proceedings of 7th Edition of the Space Propulsion Conference*, pages 1–8, 2021.
- [23] D. Maestro, Cuenot Benedicte, and Laurent Selle. Large Eddy Simulation of Combustion and Heat Transfer in a Single Element GCH₄/GO_x Rocket Combustor. *Flow Turbulence and Combustion*, 103, 09 2019.
- [24] B Marracino and D Lentini. Radiation modelling in non-luminous nonpremixed turbulent flames. *Combustion Science and Technology*, 128(1-6):23–48, 1997.
- [25] John C Melcher and Robert L Morehead. Combustion stability characteristics of the project morpheus liquid oxygen/liquid methane main engine. *AIAA Paper 2014-3681*, July 2014.
- [26] Daiki Muto, Yu Daimon, Taro Shimizu, and Hideyo Negishi. An equilibrium wall model for reacting turbulent flows with heat transfer. *International Journal of Heat Mass Transfer*, 141:1187–1195, 2019.
- [27] Nikolaos Perakis and Oskar J. Haidn. Inverse heat transfer method applied to capacitively cooled rocket thrust chambers. *International Journal of Heat Mass Transfer*, 131:150–166, 2019.
- [28] Nikolaos Perakis, Daniel Rahn, Oskar J Haidn, and Daniel Eiringhaus. Heat transfer and combustion simulation of seven-element O₂/CH₄ rocket combustor. *Journal of Propulsion and Power*, 35(6):1080–1097, 2019.
- [29] Marco Pizzarelli. An algebraic model for structural and life analysis of regeneratively-cooled thrust chambers. *Journal of Propulsion and Power*, 36(2):191–201, 2020.

CHARACTERIZATION OF INJECTORS NEAR-FIELD IN LRE

- [30] Marco Pizzarelli. Overview and analysis of the experimentally measured throat heat transfer in liquid rocket engine thrust chambers. *Acta Astronautica*, 184:46–58, 2021.
- [31] Thierry Poinso and Denis Veynante. *Theoretical and Numerical Combustion*. RT Edwards, Inc. Philadelphia, PA, USA, 2005.
- [32] Dieter Preclik, G Hagemann, O Knab, L Brummer, C Mading, D Wiedmann, and P Vuillermoz. LOX/hydrocarbon propellant trade considerations for future reusable liquid booster engines. *AIAA Paper 2005–3567*, July 2005.
- [33] Arianna Remiddi, Giuseppe Indelicato, Pasquale E Lapenna, and Francesco Creta. Thermal characterization in lre: a parametric analysis on injector arrangement. In *AIAA Paper 2021-3567*, August 2021.
- [34] Arianna Remiddi, Giuseppe Indelicato, Pasquale E Lapenna, and Francesco Creta. Effects of injector lateral confinement on lre wall heat flux characterization: numerical investigation towards data-driven modeling. In *AIAA Paper 2021-0416*, January 2021.
- [35] Gregory P Smith, David M Golden, Michael Frenklach, Nigel W Moriarty, Boris Eiteneer, Mikhail Goldenberg, CT Bowman, RK Hanson, S Song, WC Gardiner Jr, et al. Gri-mech 3.0. URL http://www.me.berkeley.edu/gri_mech, 2000.
- [36] Annafederica Urbano and Francesco Nasuti. Parametric analysis of cooling properties of candidate expander-cycle fuels. *Journal of Propulsion and Power*, 30(1):153–163, 2014.
- [37] Annafederica Urbano, Laurent Selle, Gabriel Staffelbach, Bénédicte Cuenot, Thomas Schmitt, Sébastien Ducruix, and Sébastien Candel. Exploration of combustion instability triggering using large eddy simulation of a multiple injector liquid rocket engine. *Combustion and Flame*, 169:129–140, 2016.
- [38] Jiabao Xu, Ping Jin, Ruizhi Li, Jue Wang, and Guobiao Cai. Effect of coaxial injector parameters on lox/methane engines: A numerical analysis. *Acta Astronautica*, 171:225–237, 2020.
- [39] Julian Zips, Christoph Traxinger, and Michael Pfitzner. Time-Resolved Flow Field and Thermal Loads in a Single-Element GOx/GCH4 Rocket Combustor. *International Journal of Heat Mass Transfer*, 143, 08 2019.